

# Synthesis, structural, spectroscopic, mechanical, linear and nonlinear optical studies on 4-dimethylaminopyridinium *p*-toluenesulfonate: A comparative theoretical and experimental investigation



G. Sivaraj<sup>a,b</sup>, N. Jayamani<sup>b,\*</sup>, V. Siva<sup>c,d,\*</sup>

<sup>a</sup> Department of Physics, Periyar University, Salem, 636 011, India

<sup>b</sup> Department of Physics, Government Arts College, Salem, 636 007, India

<sup>c</sup> Department of Physics, School of Advanced Sciences, Kalasalingam Academy of Research and Education, Krishnankoil, 626 126, India

<sup>d</sup> Condensed Matter Physics Laboratory, International Research Centre, Kalasalingam Academy of Research and Education, Krishnankoil, 626 126, India

## ARTICLE INFO

### Article history:

Received 3 November 2020

Revised 10 April 2021

Accepted 19 April 2021

Available online 4 May 2021

### Keywords:

Organic

Single crystal XRD

Hardness

Nonlinear optics

Quantum chemical calculations

## ABSTRACT

Single crystal of 4-(Dimethylamino)pyridinium *p*-toluenesulfonate (4DMPT) has been successfully grown by solution growth method and its structural characterization has carried out by X-ray diffraction methods. Single crystal XRD study shows that the grown crystal crystallized in the monoclinic system with unit cell dimensions  $a = 8.986$  (6) Å,  $b = 17.591$  (5) Å,  $c = 9.784$  (8) Å,  $\beta = 112.296$  (3),  $V = 1448.18$  (17) Å<sup>3</sup> and  $Z = 4$ . The quantum chemical calculations have been carried out at HF and DFT (B3LYP/CAMB3LYP/ M06-2X) with 6-311++G(d,p) levels to reach the optimized geometry, charge distributions and HOMO-LUMO nature. A good correlation is shown between computed and experimental structural parameters such as bond lengths and bond angles. The load dependent hardness values of the crystal have been analyzed. The optical spectrum revealed the ultra violet cut-off wavelength at 284 nm. The third order nonlinear optical responses have been studied by Z-Scan technique. The calculated value of third order non-linear refractive index ( $n_2$ ), third order non-linear absorption coefficient ( $\beta$ ) and third order non-linear optical susceptibility ( $\chi^{(3)}$ ) is  $8.18 \times 10^{-8}$  cm<sup>2</sup>/W,  $0.20 \times 10^{-4}$  cm/W and  $12.88 \times 10^{-6}$  esu, respectively.

© 2021 Elsevier B.V. All rights reserved.

## 1. Introduction

Nowadays, enormous efforts have been made to develop new nonlinear optical (NLO) materials due to their widespread application in technologies such as lasers, optoelectronics, frequency conversion and the optical power limiting of both organic and inorganic compounds. In organic materials, electrons are more accessible and NLO-effects arises from the interaction between light and electrons within individual molecular units, giving quicker responses [1–3]. As a part novel NLO materials synthesis, more determinations are being made to comprehend the derivation of linearity in large systems and to correlate NLO responses to molecular structure and geometry. Organic compound offers many attractive opportunities in applications which are NLO materials due to the presence of  $\pi$ -conjugated delocalized electronic structure.

Pyridinium derivatives are important in synthetic chemistry [4,5]. Among them, amino pyridines are the basic building blocks for the development of novel functional molecules. Directional hydrogen bonding interactions have strong hyperpolarizability; exhibiting non-linear optical properties [6].

Moreover, organic crystals play a crucial part in the field of supramolecular chemistry, crystal engineering and also biological sciences, etc. due to their potential applications in drug delivery and also nonlinear optics [7]. In addition, the attraction towards organic materials could be owing to ultra-fast nonlinear response time, large NLO susceptibilities moreover high laser damage threshold [8,9]. In general, several organic charges transfer crystal of *p*-toluenesulfonic acid among the organic acceptor compound revealed in NLO applications. These crystalline materials are composed of  $\pi$ -conjugated molecules chemical purity that provides highly ordered structures and a model. To explore the basic electronic properties of organic semiconductor materials, pyridine and acid are one among promising pairs forming a non-centrosymmetric crystal arrangement that exhibits high NLO performance [10–12].

\* Corresponding authors at: Department of Physics, Condensed Matter Physics Laboratory, International Research Centre, Kalasalingam Academy of Research and Education, Krishnankoil 626 126, India.

E-mail addresses: [drnjayamani@gmail.com](mailto:drnjayamani@gmail.com) (N. Jayamani), [\(V. Siva\).](mailto:siva33phy@gmail.com)

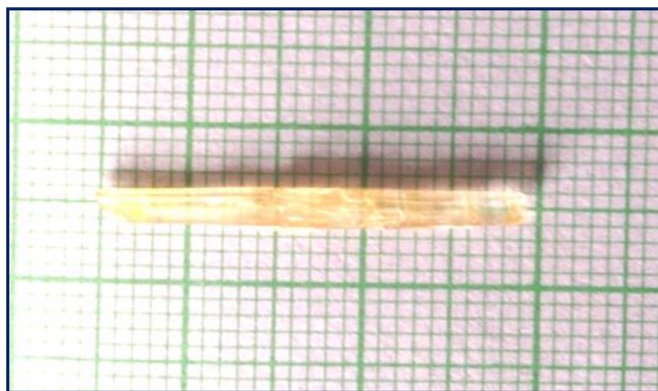


**Fig. 1.** Photograph of the 4DMPT single crystal.

The development of multi-functionalized compound with attractive physicochemical properties such as ferroelectric, ferromagnetic, piezoelectric and NLO properties for practical applications has become one of the fast growing multi-disciplinary areas [13]. 2-amino-4-picolinium toluene sulfonate [14], guanidinium p-toluenesulfonate [15,16],  $\beta$ -alaninium p-toluenesulfonate [17], L- Alaninium p- toluenesulfonate [18], L- Valinium p- toluenesulfonate monohydrate [19], L- Leucinium p- toluenesulfonate monohydrate [20] 2-Amino-5-nitropyridinium p-toluenesulfonate [21] and 2-amino 4, 6 dimethoxypyrimidine p-toluenesulfonic acid monohydrate [22] are some of the p- toluenesulfonate (tosylate) based compounds studied systematically for their NLO activity were reported previously. In this work, crystal growth, solid state properties and quantum chemical studies of 4-(dimethylamino)pyridinium p-toluenesulfonate are presented and their results are explained in detail.

## 2. Experimental and computational details

### 2.1. Synthesis and crystallization

The reactants were commercially purchased (Merck, AR Grade > 99%) and used without further purification. Solution of 4-Dimethylaminopyridine and p-toluenesulfonic acid(1:1) was heated to 40 °C and stirred for 2 h before being poured into a petri dish and kept undisturbed for 18 days. In general, the hydrogen bonds are non-bonded interactions between a positively charged hydrogen atom and an electronegative atom with lone electron pairs and can be adequately modeled by appropriately chosen atomic charges. From this reaction, the anion (p-toluenesulfonic acid) and the cation (4-dimethylaminopyridine) form a regular pattern alternating back and forth through charge transfer reaction. The crystal is held together by electrostatic attraction. Pale yellow colored single crystals were obtained by the slow evaporation of a methanol solution. The photograph of the harvested crystal was shown in Fig. 1.

### 2.2. Characterization technique details

Single crystal X-ray diffraction was used to confirm the unit cell parameters of the crystal using Bruker AXS KAPPA APEX-2 diffractometer fitted with graphite monochromator [23]. The grown crystal was analyzed to understand crystalline nature by powder XRD study using Bruker D8 advance ECO XRD systems. The Optical transmittance spectrum was measured in the range of 200–1100 nm using the UV-1700 Shimadzu spectrometer. NLO response was studied by using a Coherent Compass TM215M-50 with a wavelength of 532 nm.

**Table 1**  
Comparative representation of bond lengths for 4DMPT.

Bond length (Å)	HF	DFT			EXP
		B3LYP	CAMB3LYP	M06-2X	
C(1)–C(2)	1.361	1.374	1.368	1.374	1.363
C(1)–N(1)	1.331	1.343	1.337	1.343	1.344
C(2)–C(3)	1.419	1.422	1.416	1.422	1.425
C(3)–C(4)	1.414	1.420	1.414	1.420	1.420
C(3)–N(2)	1.343	1.358	1.352	1.358	1.336
C(4)–C(5)	1.364	1.375	1.370	1.375	1.359
C(5)–N(1)	1.334	1.346	1.341	1.346	1.342
N(2)–C(6)	1.455	1.461	1.454	1.461	1.460
N(2)–C(7)	1.456	1.461	1.455	1.461	1.461
C(10)–C(11)	1.381	1.391	1.441	1.391	1.391
C(11)–C(12)	1.387	1.393	1.385	1.393	1.394
C(11)–S(1)	1.777	1.804	1.386	1.804	1.774
C(9)–C(10)	1.388	1.394	1.789	1.394	1.392
C(8)–C(9)	1.387	1.398	1.083	1.398	1.397
C(8)–C(13)	1.393	1.400	1.393	1.400	1.382
C(8)–C(14)	1.510	1.510	1.394	1.510	1.515
C(12)–C(13)	1.381	1.391	1.505	1.391	1.391
S(1)–O(2)	1.476	1.529	1.094	1.529	1.472
S(1)–O(1)	1.453	1.488	1.457	1.488	1.450
S(1)–O(3)	1.433	1.467	1.478	1.467	1.448

### 2.3. Quantum chemical calculations

The quantum computational calculations conducted for the title compound were performed with the GAUSSIAN 09 W [24] using the DFT and HF approaches using the crystallographic data. Initially, we determined the optimized geometry within DFT using the Becke three parameter hybrid exchange functional and the Lee-Yang-Parr correlation [25–28], M06-2X and CAMB3LYP hybrid functions at 6-311++G(d,p) basis set [29–31]. The charge transfer at molecular level was assessed with a frontier molecular analysis using DFT and HF methods. Finally, the Gauss View 05 [32] was used to visualize the optimized structure, the three dimensional HOMO-LUMO images of the title compound.

## 3. Results and discussion

### 3.1. Single crystal XRD analysis

Single crystal XRD study revealed that 4DMPT ( $C_7H_{11}N_2^+$ ,  $C_7H_7O_3S^-$ ) belongs to monoclinic crystal system with space group  $P2_1/n$ . The unit cell dimensions were found to be  $a = 8.986$  (6) Å,  $b = 17.591$  (5) Å,  $c = 9.784$  (8) Å,  $\beta = 112.296$  (3),  $V = 1448.18$  (17) Å<sup>3</sup> and  $Z = 4$ . The data obtained were found to be well matched with the reported values [33]. Powder XRD pattern of 4DMPT was given in supplementary information. The crystal structure 4DMPT was formed through N–H...O and C–H...O networks of 4-dimethylaminopyridine and p-tolunesulfonic acid. Furthermore, N–H...O hydrogen bonds combined as separate pairs of cations and anions. This structure was further confirmed by the comprehensive series of C–H...O hydrogen bonds, magnified  $\pi - \pi$  [centroid-centroid distance between adjacent pyridinium rings = 3.5807 (10) Å] and C – H interactions, providing the network configuration. The structural parameters were available as crystallographic information file (CIF) at Cambridge Crystallographic Data Centre (CCDC) reference number 680683.

### 3.2. Molecular geometry

The structural parameters such as bond length and bond angle of the 4-dimethylaminopyridinium p-toluenesulfonate compound are listed in Table 1 & 2. The optimized molecular structures of title compound are depicted in Fig. 2–5 for HF and DFT (B3LYP/ CAMB3LYP/ M06-2X) with 6-311++G(d,p) levels. The comparison

**Table 2**  
Comparative representation of bond angles for 4DMPT.

Bond angle ( $^{\circ}$ )	HF	DFT			EXP
		B3LYP	CAMB3LYP	M06-2X	
C(2)–C(1)–N(1)	122.02	121.83	121.85	121.83	121.48
C(1)–C(2)–C(3)	119.47	119.79	119.66	119.79	119.56
C(2)–C(3)–C(4)	116.55	116.51	116.68	116.51	116.70
C(2)–C(3)–N(2)	121.61	121.66	121.57	121.66	121.33
C(4)–C(3)–N(2)	121.84	121.83	121.75	121.83	121.97
C(3)–C(4)–C(5)	119.97	120.22	120.12	120.22	120.08
C(1)–N(1)–C(5)	120.61	120.35	120.42	120.35	120.78
C(3)–N(2)–C(6)	120.51	120.41	120.32	120.41	120.79
C(3)–N(2)–C(7)	120.34	120.28	120.19	120.28	120.98
C(6)–N(2)–C(7)	119.15	119.31	119.49	119.31	118.20
C(10)–C(11)–C(12)	119.96	120.47	120.53	120.47	120.03
C(10)–C(11)–S(1)	120.56	120.15	120.12	120.15	119.89
C(11)–C(10)–C(9)	119.85	119.49	119.48	119.49	119.64
C(9)–C(8)–C(13)	118.32	118.24	118.36	118.24	118.39
C(9)–C(8)–C(14)	121.27	121.07	120.92	121.07	122.30
C(13)–C(8)–C(14)	120.40	120.67	120.70	120.67	119.30
C(11)–C(12)–C(13)	119.78	119.45	119.42	119.45	119.31
C(10)–C(9)–C(8)	121.01	121.16	121.08	121.16	120.97
C(8)–C(13)–C(12)	121.08	121.20	121.13	121.20	121.65
C(11)–S(1)–O(2)	105.48	104.27	106.72	104.27	104.31
C(11)–S(1)–O(1)	106.46	106.61	106.61	106.61	106.15
C(11)–S(1)–O(3)	106.65	106.81	104.53	106.81	107.29
O(2)–S(1)–O(1)	109.26	109.45	116.55	109.45	111.64
O(2)–S(1)–O(3)	112.65	112.22	112.38	112.22	114.71
O(1)–S(1)–O(3)	115.62	116.56	109.15	116.56	111.92

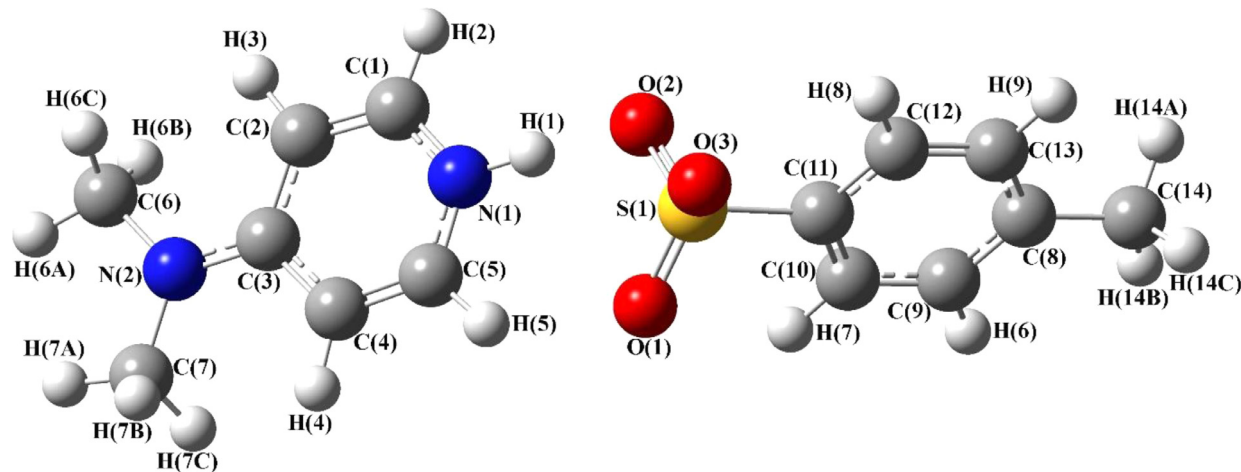


**Fig. 2.** Optimized molecular structure of 4DMPT with atom numbering scheme by HF at 6-311++G(d,p) levels.

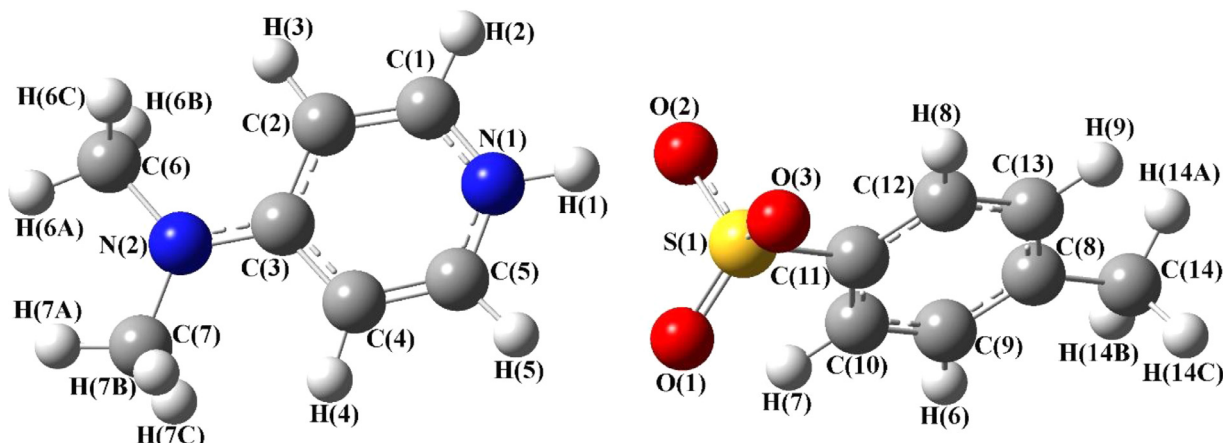


**Fig. 3.** Optimized molecular structure of 4DMPT with atom numbering scheme by B3LYP at 6-311++G(d,p) levels.

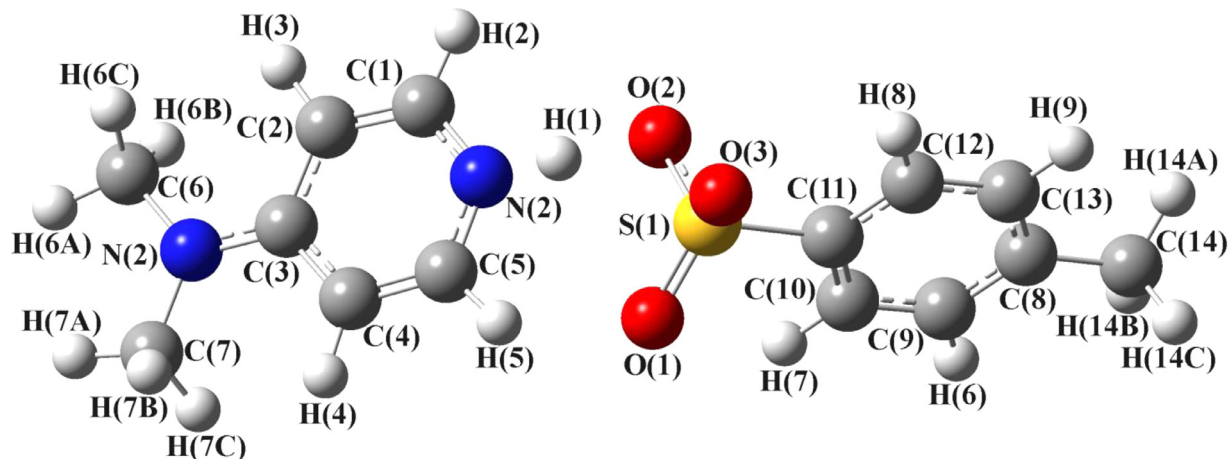


**Fig. 4.** Optimized molecular structure of 4DMPT with atom numbering scheme by CAMB3LYP at 6-311++G(d,p) levels.

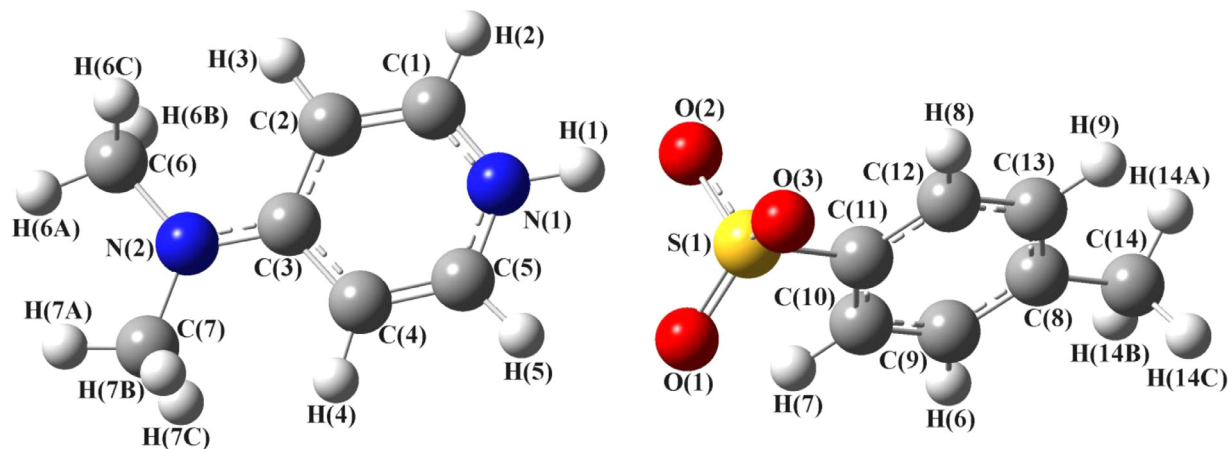


**Fig. 5.** Optimized molecular structure of 4DMPT with atom numbering scheme by M06-2X at 6-311++G(d,p) levels.

of bond angles and bond lengths of DFT with HF, showed a good agreement between the two methods with slightly larger bond lengths for the DFT values. The bond lengths of the optimized geometries are slightly higher than the experimental values and this discrepancy might be due to the fact that the calculations were performed for an isolated molecule in the gas phase and the effect of the crystalline environment was not taken into account.

The pyridine ring had two C=C bonds C(1)=C(2)=1.3606 Å / 1.374 Å (HF/DFT) and 1.363 Å (EXP), C(4)=C(5)=1.3641 Å / 1.3751 Å (HF/ B3LYP) and 1.359 Å (EXP). And two C–C single bonds C(2)–C(3)= 1.4188 Å / 1.422 Å and 1.425 Å (EXP), C(3)–C(4)= 1.4143 Å / 1.4199 Å and 1.42 Å [34], this result showed that the theoretical values were in good agreement with the experimental values.

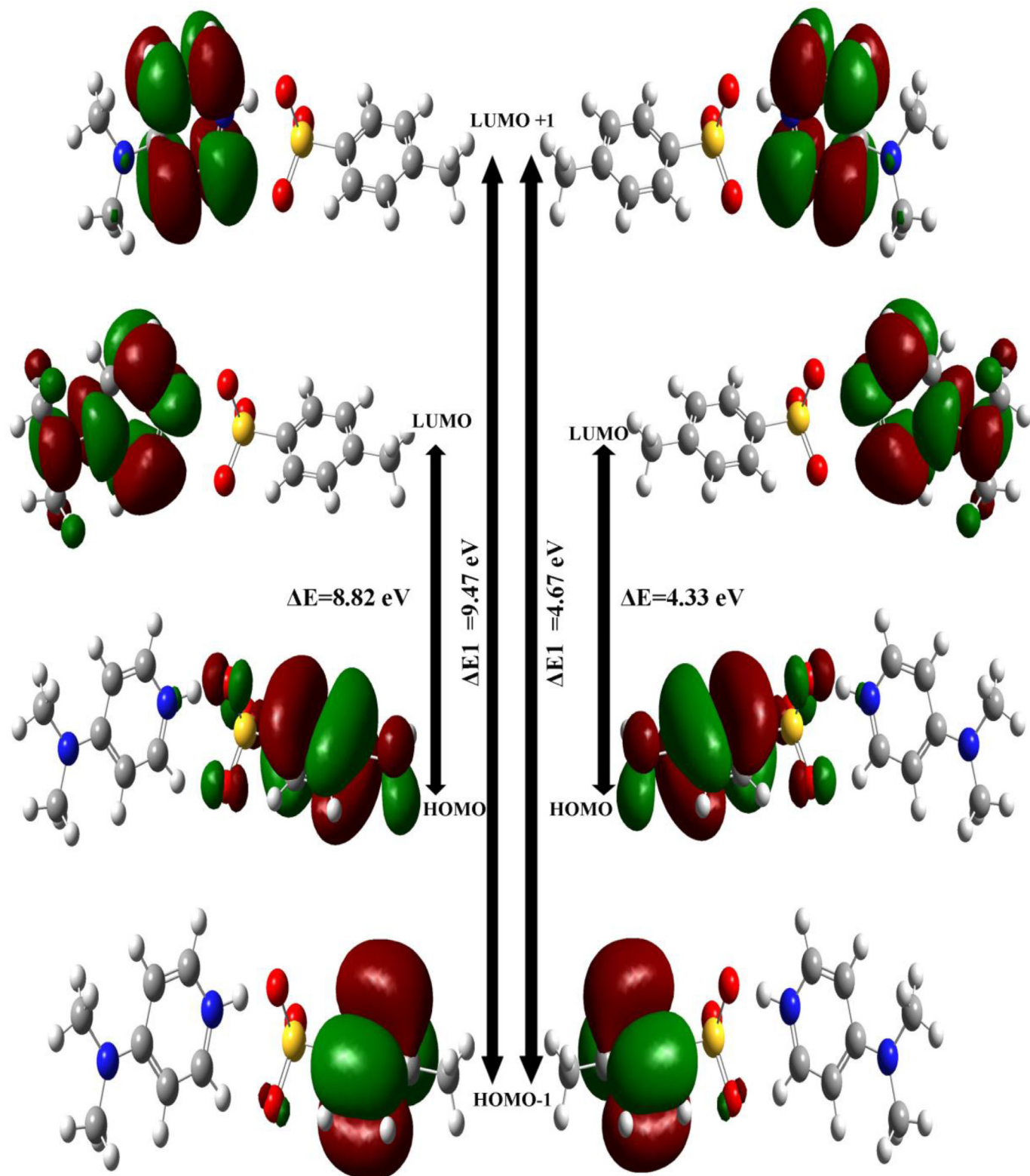
The optimized bond length of the C–N is observed and were in range of ~1.331 Å to ~1.461 Å in HF and DFT method whereas the single crystal XRD revealed that the C–N bond lengths between the range ~1.344 Å and ~1.461 Å [35,36]. The experimental results were in good agreement with the theoretical values, as it can be observed in the plots of the theoretical versus experimental geometrical parameters (given in supplementary information). The calculation provide good agreement between the theoretical and experimental bond length values except C–H and N–H bond lengths; because the calculated HF and DFT values of C–H and N–H bond lengths are lower than experimental values.

The intermolecular N–H...O hydrogen bond, the Nitrogen atom of the 4-dimethylaminopyridine and Oxygen atom of the *p*–

toluenesulfonate are observed at shorter distance in computational calculation (2.726 Å for HF, 2.824 Å/ B3LYP, 2.818 Å/ CAMB3LYP and 2.782 Å/ M06–2X for DFT methods) than the solid crystalline state (2.716 (3) Å), which is the confirmation for the dipole–dipole interaction among these two ion pairs. This result shows that the N–H...O intermolecular hydrogen bonding effect is supposed to be more between the ions in computational than solid crystalline state.

### 3.3. Frontier molecular orbitals (FMO) analysis

In FMO analysis, HOMO (Highest Occupied Molecular Orbital) and LUMO (Lowest Unoccupied Molecular Orbital) was very important to predict chemical stability. [37,38]. In order to evaluate the energetic behavior, we performed calculations on the gas phase HOMO and LUMO energy gaps calculated are presented in Table 3. The 3-D plots of the frontier orbitals shown in Fig. 6 (HF & B3LYP) and Fig. 7 (CAMB3LYP & M06–2X levels). The positive phase was red and the negative phase in green. These figures showed the electron density plot for the most important FMOs of the energy in a.u and the energy gap in the eV. The calculated energy values of HOMO = -0.3105 a.u (HF)/-0.2282 a.u (B3LYP)/ -0.2827 a.u (CAMB3LYP) /-0.2282 a.u (M06–2X) and LUMO = 0.0137 a.u (HF) / -0.0692 a.u (B3LYP) / -0.0220 a.u (CAMB3LYP) / -0.0692 a.u (M06–2X), the energy gap  $\Delta E = (E_{\text{HOMO}} - E_{\text{LUMO}})$  = 8.82 eV (HF)/ 4.33 eV (B3LYP)/ 7.1028 (CAMB3LYP) and 4.3319 (M06–2X), respectively. The energy gap ( $\Delta E$ ) was an essential parameter as a func-

**Fig. 6.** Frontier molecular orbitals by HF and DFT/B3LYP levels.

tion of the reactivity of the molecule. A molecule with a low energy gap was highly polarizable and was generally related with high chemical activity and low chemical stability and is called a soft molecule. According to Koopman's theorem [39], the energies of the HOMO and the LUMO were assigned to the ionization potential ( $I$ ), and the electron affinity ( $A$ ), respectively, by the following

relations:

$$\begin{aligned} \text{Ionization potential } (I) &= -E_{\text{HOMO}} \\ \text{Electron affinity } (A) &= -E_{\text{LUMO}} \\ \text{Electronegativity } (\chi) &= \{(I + A)/2\} \end{aligned} \quad (1)$$

$$\text{Global Hardness } (\eta) = \{(I - A)/2\} \quad (2)$$

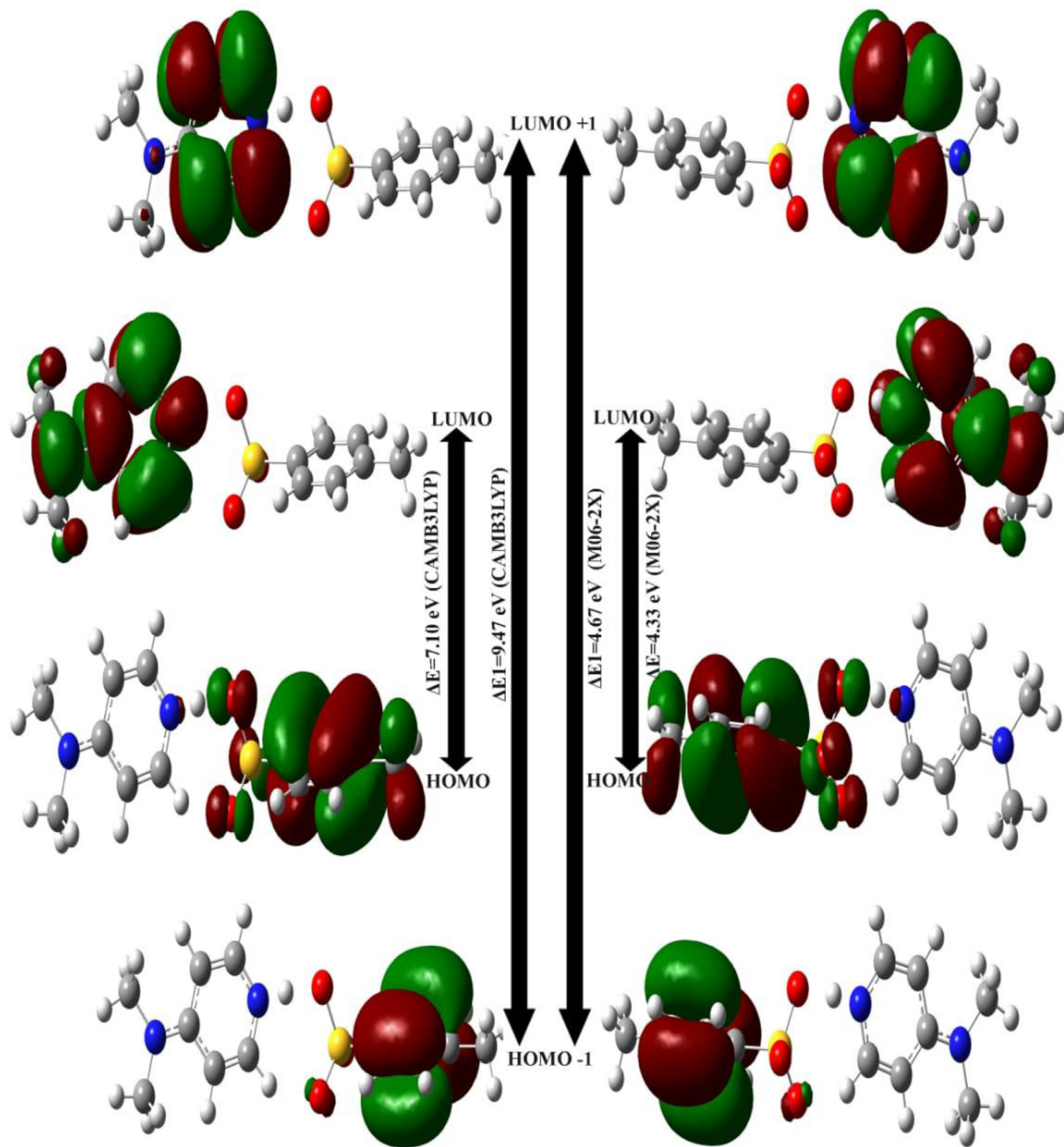


**Fig. 7.** Frontier molecular orbitals by DFT/CAMB3LYP and M06-2X levels.

$$\text{Global electrophilicity}(\omega) = (\mu^2/2\eta) \quad (3)$$

High ionization energy refers to high stability and chemical inertness and small ionization refers to the high reactivity of energy molecules. Absolute hardness and softness are important properties to measure molecular stability and reactivity. The chemical hardness refers to the resistance to decay or polarization of an electron cloud of atoms, ions, or molecules under the slightest disturbance of a chemical reaction. The NLO response of organic

molecules is often due to intra-molecular charge transfer character of FMOs and lower energy transitions which can be easily characterized by any reasonable calculation technique like DFT etc. [40].

#### 3.4. Mulliken population analysis

In Mulliken's charge analysis, each of the contributing orbitals was assigned to one another, giving the total population of each atomic orbital. Summarizing the total number of atomic orbits in a given atom was the gross atomic population [35]. The sum of

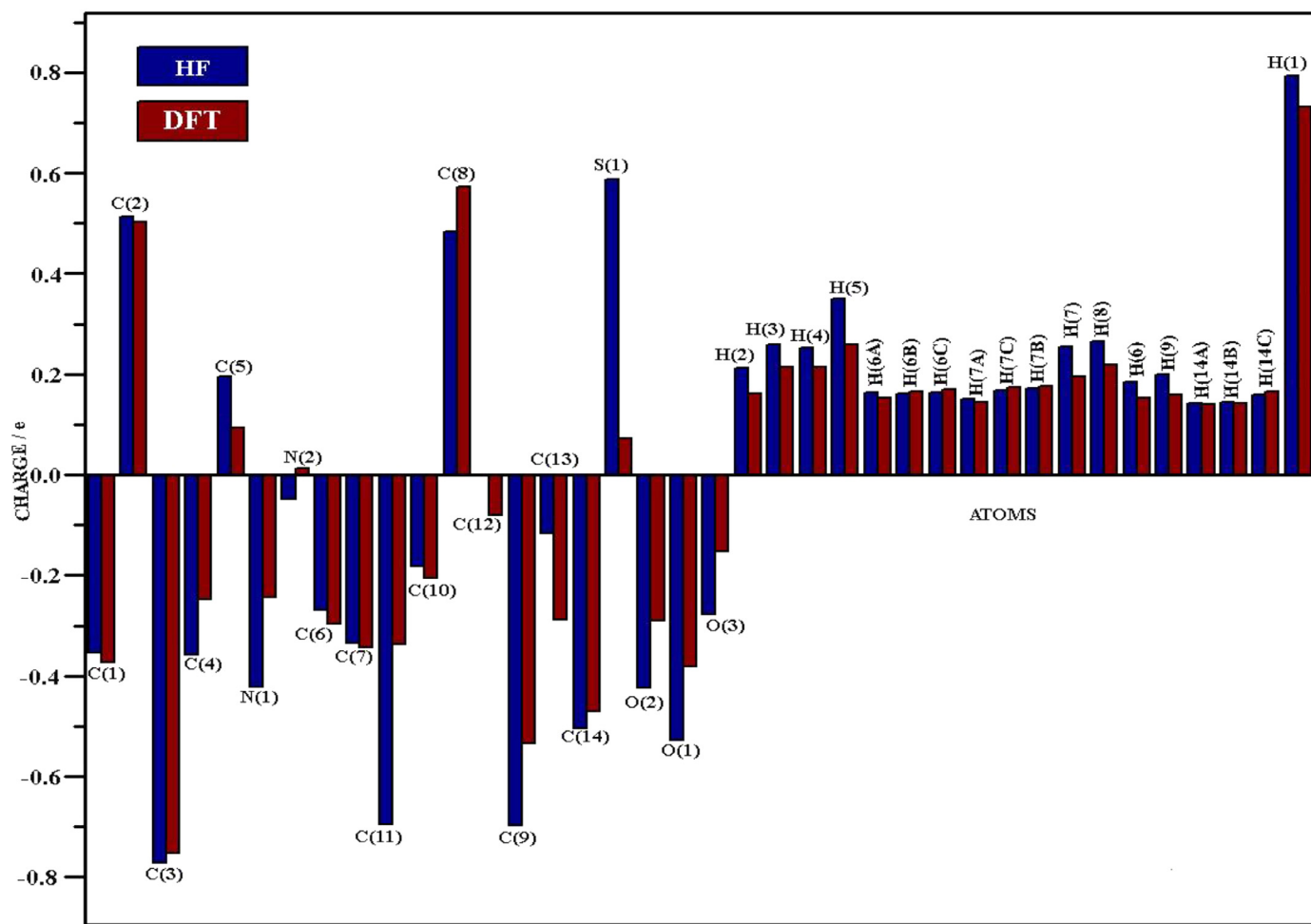


Fig. 8. Mulliken charge distributions for 4DMPT by HF and DFT/B3LYP levels.

**Table 3**  
Molecular orbital energy values of 4DMPT.

Molecular Properties	Energy				
	HF	DFT	B3LYP	CAMB3LYP	M06-2X
HOMO	-0.3105	-0.2282	-0.2827	-0.2282	
LUMO	0.0137	-0.0692	-0.0220	-0.0692	
$\Delta(E_{\text{HOMO}} - E_{\text{LUMO}})$ a.u	0.3241	0.1590	0.2607	0.1590	
$\Delta(E_{\text{HOMO}} - E_{\text{LUMO}})$ eV	8.8296	4.3310	7.1028	4.3319	
Ionization Potential (I)	0.3105	0.2282	0.2827	0.2282	
Electron Affinity (A)	-0.0137	0.0692	0.0220	0.0692	
Global Hardness ( $\eta$ )	0.1621	0.0795	0.1304	0.0795	
Global Softness ( $v$ )	6.1704	12.5794	7.6705	12.5770	
Electro negativity ( $\chi$ )	0.1484	0.1487	0.1523	0.1487	
Chemical potential ( $\mu$ )	-0.1484	-0.1487	-0.1523	-0.1487	
Global Electrophilicity ( $\omega$ )	0.0679	0.1390	0.0890	0.1390	

all net and mutual populations equals the total number of electrons in the molecule. The charge distribution on the molecule had a major influence on the vibration spectrum, dipole moment, polarization and electronic structure [41]. The Mulliken's atomic charge values were presented in Table 4 and the graphical representation was given in Figs. 8& 9. It was essential to mention that C(2), C(5) and C(8) atoms of title compound exhibit positive charges (except M06-2X), while C(1), C(3), C(4), C(6), C(7), C(11), C(10), C(12), C(9), C(13) and C(14) atoms exhibit negative charges. The C(3) atom of title compound had a

maximum negative charge value of about -0.7710(HF)/-0.7515(B3LYP)/-0.7405(CAMB3LYP)/-0.9674(M06-2X) because charge transferred from N(2) within the molecule. The C8 (0.4842 /HF, 0.5733/B3LYP, 0.5563 in CAMB3LYP) atom which was attached to the functional group ( $\text{CH}_3$ ) experienced a high positive charge, and were due to the presence of the electronegative atom, that withdraw electrons from the C atoms of the ring. All the hydrogen atoms were positive [37]. Moreover Mulliken charges showed that the H(1) atom (charge 0.7925 in HF, 0.7328 in B3LYP, 0.7113 in CAMB3LYP and 0.6370 for M06-2X) is more positive than others that is due to the hydrogen atom being surrounded by the two electronegative atoms nitrogen N(1) and oxygen O(2).

### 3.5. Mechanical stability analysis

Hardness is one of the important mechanical properties of the materials. As the hardness of the crystal determines the mechanical stability of the crystal, it was an inevitable parameter to be determined [42]. The Vicker's micro hardness polished crystals were placed on the tester's platform and fixed indentations were made using the Leitz Wetzlar Vicker's microhardness on a smooth (0 0 1) face with a constant indentation time of 10 s. Hardness number ( $H_V$ ) was determined by the relation,

$$H_V = 1.8544 P/d^2 (\text{kg/mm}^2) \quad (4)$$

Where P is the load and d is the average diagonal length of the indentation.

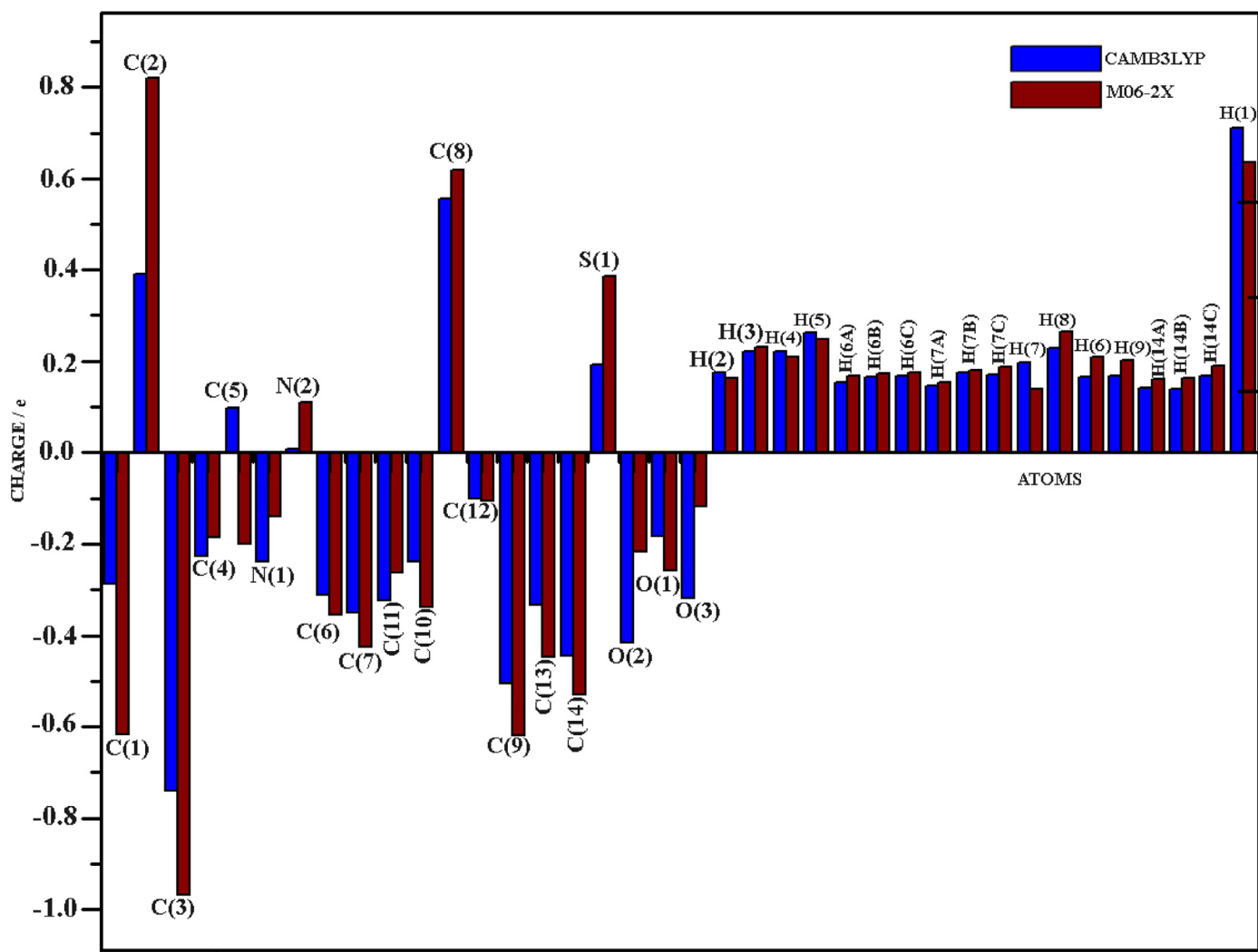
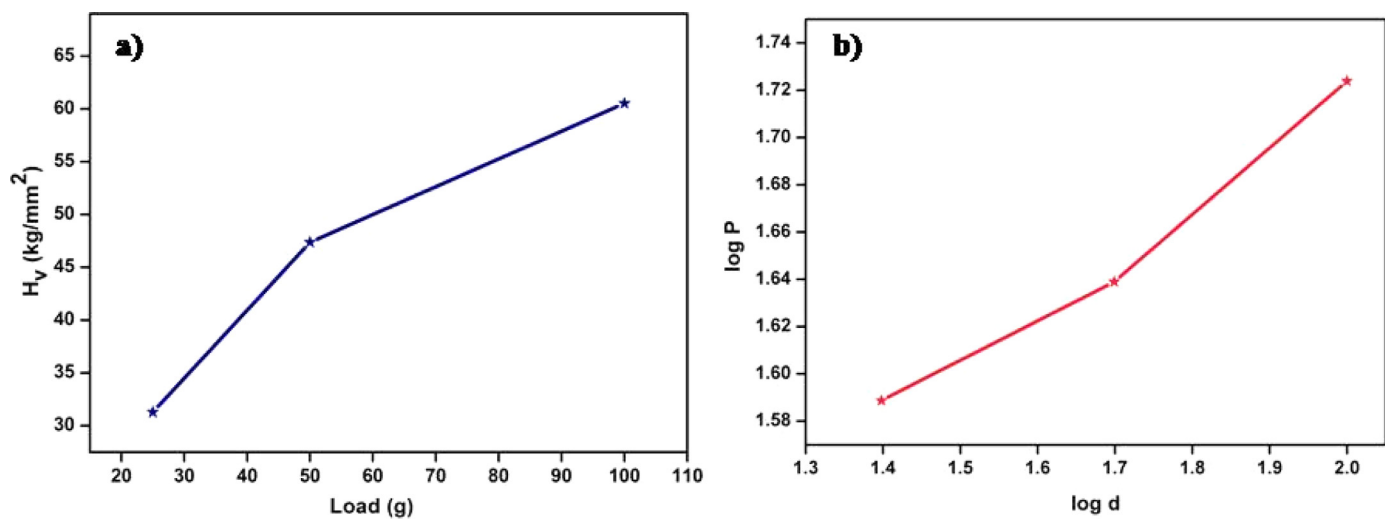


Fig. 9. Mulliken charge distributions for 4DMPT by DFT/CAMB3LYP and M06-2X levels.

Fig. 10. (a) Hardness Number ( $H_V$ ) vs Load ( $P$ ), (b) Variation of  $\log P$  with  $\log d$ .

**Table 4**  
Atomic charges of 4DMPT.

Atom	HF	DFT		
		B3LYP	CAMB3LYP	M06-2X
C(1)	-0.3541	-0.3739	-0.2886	-0.6167
C(2)	0.5128	0.5040	0.3905	0.8188
C(3)	-0.7710	-0.7515	-0.7405	-0.9674
C(4)	-0.3574	-0.2467	-0.2259	-0.1865
C(5)	0.1957	0.0937	0.0970	-0.1998
N(1)	-0.4209	-0.2430	-0.2380	-0.1398
N(2)	-0.0486	0.0132	0.0091	0.1096
C(6)	-0.2696	-0.2976	-0.3128	-0.3559
C(7)	-0.3350	-0.3440	-0.3505	-0.4258
C(11)	-0.6946	-0.3378	-0.3251	-0.2636
C(10)	-0.1833	-0.2049	-0.2398	-0.3378
C(8)	0.4842	0.5733	0.5563	0.6185
C(12)	0.0015	-0.0806	-0.1016	-0.1056
C(9)	-0.6965	-0.5337	-0.5053	-0.6182
C(13)	-0.1153	-0.2879	-0.3336	-0.4482
C(14)	-0.5040	-0.4711	-0.4458	-0.5292
S(1)	0.5866	0.0733	0.1915	0.3857
O(2)	-0.4238	-0.2905	-0.4165	-0.2162
O(1)	-0.5278	-0.3816	-0.1824	-0.2589
O(3)	-0.2767	-0.1522	-0.3181	-0.1178
H(2)	0.2119	0.1621	0.1745	0.1636
H(3)	0.2601	0.2146	0.2210	0.2314
H(4)	0.2529	0.2138	0.2223	0.2102
H(5)	0.3497	0.2593	0.2626	0.2476
H(6A)	0.1634	0.1526	0.1537	0.1688
H(6B)	0.1605	0.1663	0.1653	0.1718
H(6C)	0.1635	0.1693	0.1691	0.1760
H(7A)	0.1502	0.1439	0.1457	0.1532
H(7C)	0.1678	0.1732	0.1752	0.1809
H(7B)	0.1710	0.1753	0.1717	0.1872
H(7)	0.2550	0.1946	0.1973	0.1385
H(8)	0.2664	0.2192	0.2295	0.2646
H(6)	0.1857	0.1521	0.1652	0.2087
H(9)	0.2000	0.1599	0.1670	0.2015
H(14A)	0.1433	0.1413	0.1403	0.1597
H(14B)	0.1440	0.1427	0.1393	0.1637
H(14C)	0.1599	0.1664	0.1690	0.1903
H(1)	0.7925	0.7328	0.7113	0.6370

Fig. 10(a) showed loads with different hardness numbers and differs in that the hardness value increases with increasing load [43]. When the load reaches a maximum value of 100 g, the hardness was found to be 43.91 kg/mm<sup>2</sup>, which was found to increase the stiffness with the load. Fig. 10(b) illustrated the variation of log P with log d. The value of Meyer's index 'n' is determined from the slope of log d versus log P plot. The calculated value was 3.32, which showed the grown crystal was a soft material.

### 3.6. Linear and nonlinear optical analysis

In the UV-vis region, high transmittance had significant applications for laser threshold and optoelectronic devices. The grown crystal optical absorption spectrum was recorded in the range of 200–800 nm (Fig. 11). Absorption of organic compounds was caused by the transitions of  $\pi$  electrons to the  $\pi^*$  excited state. These electron transitions must be attributed to the molecular  $\pi$ -electrons [44]. Therefore, this transition created an absorption band over long wavelengths. The lower cut-off wavelength in grown crystal was around 298 nm in UV-Vis spectrum and had no absorption in the visible regions. This broad transparency indicated the grown crystal have the potential for a variety of optical applications [45,46].

Third order nonlinear optical parameters were analyzed on 4DMPT crystal using Z-scan technique with a length of diffraction of 1.48 mm [47,48]. Third order nonlinear parameters such as refractive index ( $n_2$ ), absorption coefficient ( $\beta$ ) and third-order NLO susceptibility ( $\chi^{(3)}$ ) of crystal was studied by Z-scan technique. The

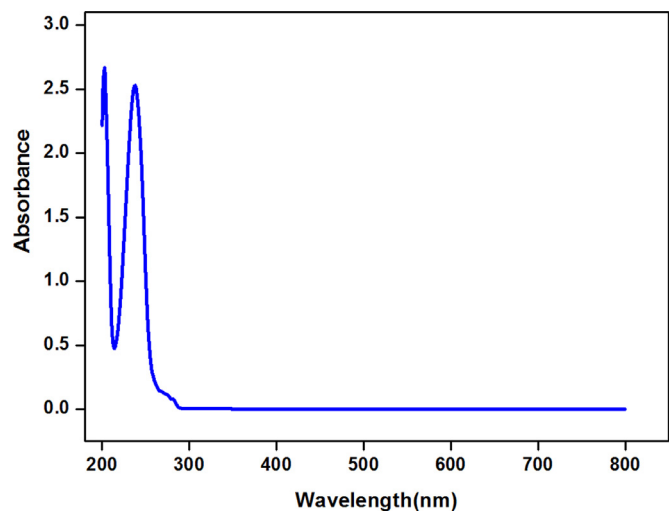


Fig. 11. Optical absorbance spectrum.

**Table 5**  
Measurement details of Z- Scan setup and calculated NLO parameters.

Parameters	Values
Laser beam wavelength( $\lambda$ )	632.8 nm
Focal length of the lens	30 mm
Optical path length	85 cm
Beam radius of the aperture ( $W_a$ )	3.3 mm
Aperture radius ( $r_a$ )	2 mm
Sample thickness ( $l$ )	0.6 mm
Beam radius ( $W_0$ )	12 $\mu$ m
Incident intensity at the focus ( $Z = 0$ )	4.38 kW/cm <sup>2</sup>
Effective thickness ( $L_{eff}$ )	0.47 mm
Linear absorption coefficient ( $\alpha$ )	0.777
Linear transmittance ( $S$ )	0.15
Nonlinear refractive index ( $n_2$ )	$8.18 \times 10^{-8}$ cm <sup>2</sup> /W
Non linear absorption coefficient ( $\beta$ )	$0.20 \times 10^{-4}$ cm/W
Third order nonlinear susceptibility ( $\chi^{(3)}$ )	$12.88 \times 10^{-6}$ esu

real and imaginary parts of the third order Non-linear optical susceptibility  $\chi^{(3)}$  were defined as

$$\text{Re } \chi^{(3)} = (10^{-4} \times \varepsilon_0 c^2 n_0^2 n_2) / \pi \quad (5)$$

$$\text{Im } \chi^{(3)} = (10^{-2} \times \varepsilon_0 c^2 n_0^2 \lambda \beta) / (4\pi^2) \quad (6)$$

where  $\varepsilon_0$  is the vacuum permittivity,  $n_0$  is the linear refractive index of the sample and  $c$  is the velocity of light in vacuum. The absolute value of the third order Non-linear optical susceptibility  $\chi^{(3)}$  was calculated from the formula

$$\chi^{(3)} = \left[ (\text{Re } \chi^{(3)})^2 + (\text{Im } \chi^{(3)})^2 \right]^{1/2} \quad (7)$$

The calculated value of third order non-linear refractive index ( $n_2$ ), third order non-linear absorption coefficient ( $\beta$ ) and the third order non-linear optical susceptibility ( $\chi^{(3)}$ ) is  $8.18 \times 10^{-8}$  cm<sup>2</sup>/W,  $0.20 \times 10^{-4}$  cm/W and  $12.88 \times 10^{-6}$  esu, respectively.

The measurement details of Z- Scan setup and calculated NLO parameters were given in Table 5. The decrease in normalized transmittance with the input intensity suggested that reverse saturation absorption was the leading mechanism behind non-linear absorption in crystals. According to these results, to achieve saturated absorption, low intensity energy levels must be filled up to the level of photon excitation [49,50]. The results of the title compound have been compared with some of the reported p-toluenesulfonate crystals and are presented in Table 6. It suggests that the grown crystal possess higher ( $\chi^{(3)}$ ) value than the reported p-toluenesulfonate materials. With the above characteris-

**Table 6**

Comparison of nonlinear absorption coefficient and nonlinear optical susceptibility with some of the *p*-toluenesulfonate crystals.

Material	Third order nonlinear absorption coefficient ( $\beta$ ) (cm/W)	Third order nonlinear susceptibility $\chi^{(3)}$ (esu)	Ref.
2-amino-4-picolinium toluene sulfonate	$-7.7 \times 10^{-4}$	$3.38 \times 10^{-6}$	[14]
Guanidinium <i>p</i> -toluenesulfonate	$0.08 \times 10^{-4}$	$2.74 \times 10^{-6}$	[16]
$\beta$ -alaninium <i>p</i> -toluenesulfonate	$2.329 \times 10^{-2}$	$7.372 \times 10^{-11}$	[17]
2-amino 4, 6 dimethoxy pyrimidine <i>p</i> -toluenesulfonic acid monohydrate	$0.311 \times 10^{-2}$	$3.143 \times 10^{-4}$	[21]
4-dimethylaminopyridinium <i>p</i> -toluenesulfonate	<b><math>0.20 \times 10^{-4}</math></b>	<b><math>12.88 \times 10^{-6}</math></b>	<b>Present work</b>

tics, title compound can be declared as an excellent candidate for optoelectronic device applications.

#### 4. Conclusions

Optically good quality single crystals of 4DMPT were successfully grown by slow evaporation method. The structural parameters of grown crystal were characterized by single-crystal X-ray diffraction. Hardness test showed that 4DMPT belong to the soft material category. FMO energy gap values of the 4DMPT demonstrated the charge transfer interactions that took place within the crystal lattice and the strong N-H...O, O-H...O and hydrogen bonding had also been confirmed. The charge distributions were calculated by the Mulliken population analysis. The UV-Visible absorption spectrum indicated that the crystal was suitable for NLO applications. The lower cut-off wavelength in grown crystal was around 298 nm in UV-Vis absorbance spectrum. Third order nonlinear optical susceptibility value was found to be  $12.88 \times 10^{-6}$  esu. Optical transparency and large nonlinear optical susceptibility of grown crystal demonstrated its suitability for various optoelectronic device applications.

#### Declaration of Competing Interest

None.

#### Supplementary materials

Supplementary material associated with this article can be found, in the online version, at doi:[10.1016/j.molstruc.2021.130530](https://doi.org/10.1016/j.molstruc.2021.130530).

#### CRediT authorship contribution statement

**G. Sivaraj:** Conceptualization, Writing – original draft. **N. Jayamani:** Supervision. **V. Siva:** Validation.

#### References

- B.M. Sornamurthy, G. Peramaiyan, P. Rekha, R.Mohan Kumar, V. Manivannan, Growth, structural, thermal, optical, dielectric, mechanical and laser damage threshold studies of nicotinium tartrate single crystals, Optik 125 (2014) 5695–5700, doi:[10.1016/j.ijleo.2014.06.091](https://doi.org/10.1016/j.ijleo.2014.06.091).
- S. Suresh, The Growth and the Optical, Mechanical, Dielectric and Photoconductivity Properties of a New Nonlinear Optical Crystal- L-Phenylalanine-4-nitrophenol NLO Single Crystal, J. Crys. Pro. Tech. 3 (2013) 87–91, doi:[10.4236/jcpt.2013.33014](https://doi.org/10.4236/jcpt.2013.33014).
- V. Siva, S. Asath Bahadur, A. Shameem, A. Murugan, S. Athimoolam, M. Suresh, Synthesis, supramolecular architecture, thermal and optical behavior of 4-methoxy anilinium perchlorate: a promising third-order NLO material for optical limiting device applications, Opt. Mater. 96 (2019) 109290, doi:[10.1016/j.optmat.2019.109290](https://doi.org/10.1016/j.optmat.2019.109290).
- S. Krishnan, C. Justin Raj, S. Dinakaran, R. Utharakumar, R. Robert, S. Jerome Das, Optical, thermal, dielectric and ferroelectric behaviour of sodium acid phthalate (SAP) single crystals, J. Phys. Chem. Solid. 69 (2008) 2883–2887, doi:[10.1016/j.jpcs.2008.06.146](https://doi.org/10.1016/j.jpcs.2008.06.146).
- K. Ramachandran, A. Raja, V. Mohankumar, M. Senthil Pandian, P. Ramasamy, Experimental and theoretical approach of organic 4,4'-dimethylbenzophenone (DMBP) single crystal for NLO application, Opt. Laser Technol. 119 (2019) 105640, doi:[10.1016/j.optlastec.2019.105640](https://doi.org/10.1016/j.optlastec.2019.105640).
- V. Siva, S. Asath Bahadur, A. Shameem, S. Athimoolam, K. Udaya Lakshmi, G. Vinitha, Synthesis, structural, vibrational, thermal, dielectric and optical properties of third order nonlinear optical single crystal for optical power limiting applications, J. Mol. Struct. 1191 (2019) 110–117, doi:[10.1016/j.molstruc.2019.04.091](https://doi.org/10.1016/j.molstruc.2019.04.091).
- S. Muhammad, M. Nakano, A.G. Al-Sehemi, Y. Kitagawa, A. Irfan, A.R. Chaudhry, K. Fukuda, Role of a singlet diradical character in carbon nanomaterials: a novel hot spot for efficient nonlinear optical materials, Nanoscale 8 (42) (2016) 17998–18020.
- S. Muhammad, H.-L. Xu, R.-L. Zhong, Z.-M. Su, A.G. Al-Sehemi, A. Irfan, Quantum chemical design of nonlinear optical materials by sp<sub>2</sub>-hybridized carbon nanomaterials: issues and opportunities, J. Mater. Chem. C 1 (35) (2013) 5439.
- S. Muhammad, M. Nakano, Computational strategies for nonlinear optical properties of carbon nano-systems, Nanosci. Comput. Chem. (2013) Apple Academic Press, New York.
- A. Anandhan, C. Sivasankari, M. Saravanabhan, V. Siva, K. Senthil, Synthesis, crystal structure, spectroscopic investigations, physicochemical properties of third order NLO single crystal for optical applications, J. Mol. Struct. (2019) 127400.
- G. Vadivelan, M. Saravanabhan, V. Murugesan, M. Sekar, Synthesis, characterization and biological studies of a charge transfer complex: 2-aminopyridinium-4-methylbenzenesulfonate, Spectrochim. Acta A 145 (2015) 461–466, doi:[10.1016/j.saa.2015.03.045](https://doi.org/10.1016/j.saa.2015.03.045).
- M. Odabas,oglu, O. Buyukgunor, G. Turgut, A. Karada ğ, E. Bulak, P.L. onnecke, Crystal structure, spectral and thermal properties of 2-aminopyridinium adipate monoacidic acid dehydrate, J. Mol. Struct. 648 (2003) 133–138, doi:[10.1016/S0022-2860\(02\)00720-2](https://doi.org/10.1016/S0022-2860(02)00720-2).
- R. Chitra, R.R. Choudhury, T. Vijay, M.V. Hosur, Guru T.N. Row, Molecular interactions in bis(2-aminopyridinium) malonate: a crystal isostructural to bis(2-aminopyridinium) maleate crystal, J. Mol. Struct. 1010 (2012) 46–51, doi:[10.1016/j.molstruc.2011.11.017](https://doi.org/10.1016/j.molstruc.2011.11.017).
- G.Anandha Babu, P. Ramasamy, Growth and characterization of 2-amino-4-picolinium toluene sulfonate single crystal, Spectrochimica Acta 2 (1) (2011) 521–526, doi:[10.1016/j.saa.2011.08.003](https://doi.org/10.1016/j.saa.2011.08.003).
- Paavai Era, RoMu Jauhar, P. Vivek, P. Murugakoothan, Investigation on the optical, electronic, mechanical and thermal parameters of guanidinium *p*-toluenesulfonate single crystal for opto-electronic applications, Mater. Chem. Phys. 257 (2021) 123647, doi:[10.1016/j.matchemphys.2020.123647](https://doi.org/10.1016/j.matchemphys.2020.123647).
- Paavai Era, RO.MU. Jauhar, G. Vinitha, P. Murugakoothan, Synthesis, growth, structural modeling and physio-chemical properties of a charge transfer molecule: guanidinium tosylate, Opt. Laser Technol. 101 (2018) 127–137, doi:[10.1016/j.optlastec.2017.11.005](https://doi.org/10.1016/j.optlastec.2017.11.005).
- M. Suresh, V. Siva, S. Asath Bahadur, S. Athimoolam, Structural elucidation, hydrogen bonding motifs and solid state properties of *p*-toluenesulfonate salt of  $\beta$ -alanine for optoelectronic device application, J. Mol. Struct. 1221 (2020) 128820, doi:[10.1016/j.molstruc.2020.128820](https://doi.org/10.1016/j.molstruc.2020.128820).
- M. Suresh, S. Asath Bahadur, S. Athimoolam, Synthesis, growth and characterization of a new hydrogen bonded organic tosylate crystal: L-Alanine *p*-toluenesulfonate for second order nonlinear optical applications, J. Mater. Sci. 27 (5) (2016) 4578–4589.
- M. Suresh, S. Asath Bahadur, S. Athimoolam, Synthesis, Growth, structural, spectral, thermal and microhardness studies of a new hydrogen bonded organic nonlinear optical material: L-Valinium *p*-toluenesulfonate monohydrate (LVPT), J. Mol. Struct. 1112 (2016) 71–80.
- M. Suresh, S. Asath Bahadur, S. Athimoolam, Structural and solid state prop-

- erties of L-Leuinium p-toluenesulfonate monohydrate: an amino acid tosylate NLO crystal, *J. Mater. Sci.* **28** (1) (2017) 661–672.
- [21] G. Anandha Babu, R. Perumal Ramasamy, P. Ramasamy, V. Krishna Kumar, Synthesis, Crystal Growth, and Characterization of an Organic Nonlinear Optical Donor- $\pi$ -Acceptor Single Crystal: 2-Amino-5-nitropyridinium-Toluenesulfonate, *Cryst. Growth Des.* **9** (2009) 3333–3337, doi:[10.1021/cg9001384](https://doi.org/10.1021/cg9001384).
- [22] RO.MU. Jauhar, S. Kalainathan, P. Murugakoothan, Three dimensional organic framework of 2-amino 4, 6 dimethoxypyrimidine p-toluenesulfonic acid monohydrate: synthesis, single crystal growth and its properties, *J. Cryst. Growth* **424** (2015) 42–48, doi:[10.1016/j.jcrysgro.2015.05.003](https://doi.org/10.1016/j.jcrysgro.2015.05.003).
- [23] Bruker, SAINT, SMART, Brucker AXS Inc, Madison, Wisconsin, USA, 2001.
- [24] M.J. Frisch, G.W. Trucks, H.B. Schlegel, G.E. Scuseria, M.A. Robb, J.R. Cheeseman, G. Scalmani, V. Barone, B. Mennucci, G.A. Petersson, H. Nakatsuji, M. Caricato, X. Li, H.P. Hratchian, A.F. Izmaylov, J. Bloino, G. Zheng, J.L. Sonnenberg, M. Hada, M. Ehara, K. Toyota, R. Fukuda, J. Hasegawa, M. Ishida, T. Nakajima, Y. Honda, O. Kitao, H. Nakai, T. Vreven, J.A. Montgomery Jr., J.E. Peralta, F. Ogliaro, M. Bearpark, J.J. Heyd, E. Brothers, K.N. Kudin, V.N. Staroverov, R. Kobayashi, J. Normand, K. Raghavachari, A. Rendell, J.C. Burant, S.S. Iyengar, J. Tomasi, M. Cossi, N. Rega, J.M. Millam, M. Klene, J.E. Knox, J.B. Cross, V. Bakken, C. Adamo, J. Jaramillo, R. Gomperts, R.E. Stratmann, O. Yazyev, A.J. Austin, R. Cammi, C. Pomelli, J.W. Ochterski, R.L. Martin, K. Morokuma, V.G. Zakrzewski, G.A. Voth, P. Salvador, J.J. Dannenberg, S. Dapprich, A.D. Daniels, O. Farkas, J.B. Foresman, J.V. Ortiz, J. Cioslowski, D.J. Fox, Gaussian 09, Revision B.01, Gaussian Inc., Wallingford, 2010.
- [25] R.G. Parr, W. Yang, Density-Functional Theory of Atoms and Molecules, Oxford University Press, 1989.
- [26] W. Koch, M.C. Holthausen, A Chemist's Guide to Density Functional Theory, Wiley-VCH, Weinheim, 2000.
- [27] D. Young, Computational Chemistry: A Practical Guide for Applying Techniques to Real World Situations, Wiley, USA, 2001.
- [28] C.J. Cramer, Essentials of Computational Chemistry, Wiley, USA, 2003.
- [29] T. Seidler, K. Stadnicka, B. Champagne, Evaluation of the linear and second-order NLO properties of molecular crystals within the local field theory: electron correlation effects, choice of XC functional, PVPA contributions, and impact of the geometry in the case of 2-methyl-4- nitroaniline, *J. Chem. Theory Comput.* **10** (2014) 2114–2124.
- [30] L.E. Johnson, L.R. Dalton, B.H. Robinson, Optimizing Calculations of Electronic Excitations and Relative Hyperpolarizabilities of Electrooptic Chromophores, *Acc. Chem. Res.* **47** (11) (2014) 3258–3265.
- [31] P.S. Pereira da Silva, P. Martín-Ramos, S.R. Domingos, M. do Carmo Bota de Sousa, C.T. Arranja, Abílio J.F.N. Sobral, M.R. Silva, On the performance of hybrid functionals for nonlinear optical properties and electronic excitations in chiral molecular crystals: the case of butterfly-shaped dicinnamalacetone, *Chem. Phys. Chem.* **19** (2018) 82–92.
- [32] R. Dennington, T. Keith, J. Millam, Gauss View Version 5.0.8 Semichem Inc, Shawnee Mission KS, 2013.
- [33] C.John McAdam, Jim Simpson, 4-(Dimethylamino)pyridinium 4-toluenesulfonate, *Acta Cryst. E64* (2008) o627–o628, doi:[10.1107/S1600536808004856](https://doi.org/10.1107/S1600536808004856).
- [34] V. Siva, M. Suresh, S. Athimoolam, S. Asath Bahadur, Crystal structure and Hirshfeld surface analysis of 2-aminopyridinium hydrogen phthalate, *Acta Crystallogr. Sect. E75* (2019) 1627–1631.
- [35] V. Siva, S. Suresh Kumar, M. Suresh, M. Raja, S. Athimoolam, S. Asath Bahadur, N-H...O hydrogen bonded novel nonlinear optical semiorganic crystal (4-methoxyanilinium trifluoroacetate) studied through theoretical and experimental methods, *J. Mol. Struct.* **1133** (2017) 163–171.
- [36] G. Sivaraj, N. Jayamani, V. Siva, Structural, spectroscopic, physical properties and quantum chemical investigation on bromide salt of 4-dimethylaminopyridine NLO material for optoelectronic applications, *J. Mol. Struct.* **1216** (2020) 128242, doi:[10.1016/j.molstruc.2020.128242](https://doi.org/10.1016/j.molstruc.2020.128242).
- [37] S. Thangarasu, V. Siva, S. Athimoolam, S. Asath Bahadur, Molecular structure, spectroscopic and quantum chemical studies on benzoic acid and succinic acid co-crystals of 2-Aminopyrimidine, *J. Theo. Comp. Chem.* **174** (2018) 1850021.
- [38] V. Siva, A. Shameem, S. Suresh Kumar, M. Raja, S. Athimoolam, S. Asath Bahadur, Structural, spectral, Quantum chemical and thermal studies on a new NLO crystal: guanidinium Cinnamate, *J. Mater Sci: Mater Electron.* **28** (17) (2017) 12484–12496.
- [39] M.V. Putz, Koopmans' Analysis of Chemical Hardness with Spectral-Like Resolution, *Sci. World J.* (2013) 1–14, doi:[10.1155/2013/348415](https://doi.org/10.1155/2013/348415).
- [40] S. Muhammad, M. Shkhir, S. AlFaify, A. Irfan, A.G. Al-Sehem, Combined experimental and computational insights into the key features of L-alanine L-alaninium picrate monohydrate: growth, structural, electronic and nonlinear optical properties, *RSC Adv.* **5** (2015) 53988–54002.
- [41] P. Karthiga Devi, K. Venkatachalam, Growth, spectroscopic, mechanical, thermal, antimicrobial and DFT studies of piperidinium hydrogen oxalate, *J. Mater. Sci.* **28** (2017) 8061–8073, doi:[10.1007/s10854-017-6512-7](https://doi.org/10.1007/s10854-017-6512-7).
- [42] V. Siva, A. Shameem, A. Murugan, M. Anandha Jothi, M. Suresh, S. Athimoolam, S. Asath Bahadur, Structural, mechanical, thermal, electro-optical studies on diprotonated adipate salt of para-anisidine for intensity tunable optical limiting applications, *J. Mater. Sci.* **31** (2017) 17921–17930, doi:[10.1007/s10854-020-04344-0](https://doi.org/10.1007/s10854-020-04344-0).
- [43] F. Helen, G. Kanchana, Growth, mechanical, dielectric, thermal and optical studies of a nonlinear optical crystal: L-Histidinium dipicrate dehydrate, *J. Mat. Chem. Phys.* **151** (2015) 5–13, doi:[10.1016/j.matchemphys.2014.11.064](https://doi.org/10.1016/j.matchemphys.2014.11.064).
- [44] P. Karthiga Devi, K. Venkatachalam, Growth, spectroscopic, optical, thermal, dielectric and DFT studies of ammonium picrate: a nonlinear optical crystal, *J. Mat. Sci.* **27** (8) (2016) 8590–8598, doi:[10.1007/s10854-016-4877-7](https://doi.org/10.1007/s10854-016-4877-7).
- [45] F. Helen, G. Kanchana, V. Siva, Structural investigation, thermal, electrical and optical properties of NLO active single crystal for optoelectronic device applications, *J. Mat. Sci.* **31** (2020) 17158–17172, doi:[10.1007/s10854-020-04248-z](https://doi.org/10.1007/s10854-020-04248-z).
- [46] N. Bhuvaneswari, N. Priyadarsini, S. Sivakumar, K. Venkatachalam, V. Siva, Growth, vibrational, optical, thermal, magnetic and dielectric behavior of organo-metallic tetramethyl ammonium cadmium chloride crystal, *J. Therm. Anal Calorim* **136** (2018) 411–417.
- [47] J. Yi, L. Miao, J. Li, W. Hu, C. Zhao, S. Wen, Third-order nonlinear optical response of  $\text{CH}_3\text{NH}_3\text{PbI}_3$  perovskite in the mid-infrared regime, *Opt. Mater. Express* **7** (2017) 3895, doi:[10.1364/OME.7.003894](https://doi.org/10.1364/OME.7.003894).
- [48] O. Muller, V. Pichot, L. Merlat, D. Spitzer, Optical limiting properties of surface functionalized nanodiamonds probed by the Z-scan method, *Sci. Rep.* **9** (2019) 519, doi:[10.1038/s41598-018-36838-7](https://doi.org/10.1038/s41598-018-36838-7).
- [49] V. Siva, A. Shameem, A. Murugan, S. Athimoolam, M. Suresh, S. Asath Bahadur, A promising guanidinium based metal-organic single crystal for optical power limiting applications, *Chine. J. Phys.* **64** (2020) 103–114, doi:[10.1016/j.cjph.2020.01.001](https://doi.org/10.1016/j.cjph.2020.01.001).
- [50] S. Zongo, K. Sanusi, J. Britton, P. Mthunzi, T. Nyokong, M. Maaza, B. Sahraoui, Nonlinear optical properties of natural laccaic acid dye studied using Z-scan technique, *Opt. Mater.* **46** (2015) 270–275, doi:[10.1016/j.optmat.2015.04.031](https://doi.org/10.1016/j.optmat.2015.04.031).